1 **Bariatric surgery reveals a gut-restricted TGR5 agonist that exhibits anti-diabetic effects**

2

3 Snehal N. Chaudhari[1#], David A. Harris[2#], Hassan Aliakbarian [2], Matthew T. Henke[1], Renuka

4 Subramaniam[2], Ashley H. Vernon[2], Ali Tavakkoli[2], Eric G. Sheu[2*], A. Sloan Devlin[1*]

5

6 [#]Co-first author   *Co-corresponding author

7 [1]Department of Biological Chemistry and Molecular Pharmacology, Harvard Medical School,

8 Boston, MA, 02115

9 [2]Department of Surgery, Brigham and Women's Hospital, Harvard Medical School, Boston, MA

10

11 Correspondence: esheu@bwh.harvard.edu, sloan_devlin@hms.harvard.edu

12

13

14

15
16

Abstract

Bariatric surgery, the most effective treatment for obesity and type 2 diabetes, is consistently associated with increased levels of the incretin hormone GLP-1 and changes in overall levels of circulating bile acids. The levels of individual bile acids in the GI tract following surgery, however, have remained largely unstudied. Using UPLC-MS-based quantification, we observed an increase in an endogenous bile acid, cholic acid-7-sulfate (CA7S), in the GI tract of both mice and humans after sleeve gastrectomy. We show that CA7S is a TGR5 agonist that induces GLP-1 secretion in vitro and in vivo and that CA7S administration increases glucose tolerance in insulin-resistant mice in a GLP-1 receptor-dependent manner. CA7S remains gut-restricted, minimizing off-target effects previously observed for TGR5 agonists absorbed into circulation. By studying changes in individual metabolites following surgery, this study has revealed a naturally occurring TGR5 agonist that exerts systemic glucoregulatory effects while remaining confined to the gut.

Introduction

Obesity and type 2 diabetes (T2D) are medical pandemics. Bariatric surgery, in the form of Roux-en-Y gastric bypass or sleeve gastrectomy (SG), is currently the most effective and lasting treatment for obesity and related comorbidities[1,2]. For a majority of patients, remission is durable and lasts for years after surgery[1,3]. Two changes consistently observed following bariatric surgery are increased levels of GLP-1, a circulating incretin hormone, and changes in the systemic repertoire of bile acids[4]. Bile acids are cholesterol-derived metabolites that play crucial roles in host metabolism by acting as detergents that aid in the absorption of lipids and vitamins, and as ligands for host receptors[5]. Bile acids have been implicated in post-SG therapeutic benefits due to their ability to mediate signaling through the G protein-coupled bile acid receptor (GPBAR1, also known as TGR5)[6] and the farnesoid X receptor (FXR)[7]. Thus far, research efforts have focused on overall changes in the total bile acid pool or in levels of conjugated or unconjugated bile acids in circulating blood[4,8]. Individual bile acids, however, have different binding affinities for

43   nuclear hormone receptors (NhRs) and GPCRs, and thus unique abilities to modulate glucose

44   homeostasis, lipid accumulation, and energy expenditure[5,9]. It is not sufficient, therefore, to limit

45   analyses to whole classes of bile acids. Moreover, local activation of receptors in the intestine can

46   affect global metabolic outcomes. In particular, GLP-1 is secreted post-prandially by

47   enteroendocrine L cells in the lower intestine in response to activation of TGR5, a G-protein

48   coupled receptor with a primary role in energy metabolism[10]. GLP-1 directly stimulates pancreatic

49   insulin release, and both hormones then regulate metabolism systemically [11]. In this work, we

50   sought to identify specific naturally occurring bile acids whose levels were increased in the gut

51   following SG and then to investigate the role of these compounds as potential TGR5 ligands and

52   thus regulators of glucose metabolism. We identified one bile acid, cholic acid-7-sulfate (CA7S),

53   whose levels were increased in cecal contents and feces of mice and humans, respectively, after

54   SG. We then determined that CA7S is a gut-restricted TGR5 agonist and GLP-1 secretagogue

55   that increases acute glucose tolerance when administered to diet-induced obese mice.

56

57   **Results**

58   **Intestinal bile acid profiling reveals increased CA7S in mice and humans post-SG**

59   Owing to robust post-surgical metabolic benefits and favorable side-effect profile, SG is the most

60   common bariatric surgery performed in the US[12]. Rodent SG models mimic the positive metabolic

61   outcomes observed in humans and are thus suitable for studying post-surgical outcomes[13]. In this

62   study, SG or sham surgery was performed on insulin-resistant, diet-induced obese (DIO) mice

63   (Fig. 1a). SG mice displayed improved glucose tolerance and insulin sensitivity 4-5 weeks post-

64   surgery compared to shams (Fig. 1b-e). Mice were euthanized six weeks post-surgery and their

65   tissues were harvested. Consistent with studies involving human patients[4], we observed an

66   increase in circulating GLP-1 in SG mice (Fig. 1f). Individual bile acids that are known agonists of

67   TGR5 have been shown to induce GLP-1 secretion in lower-intestinal L cells[4,10]. We therefore

68   quantified individual bile acids in cecal contents of SG and sham mice using Ultra-high

3

69   Performance Liquid Chromatography-Mass Spectrometry (UPLC-MS) (Fig. 2a). We observed a

70   significant increase in only one bile acid in cecal contents of SG mice. Based on its mass, this

71   compound appeared to be a monosulfated metabolite of a trihydroxy bile acid. We purified this

72   compound from pooled extracts of post-SG cecal contents using mass spectrometry-guided semi-

73   preparative HPLC. Using NMR spectroscopy, we then identified this compound as cholic acid-7-

74   sulfate (CA7S) (Fig. 2b,c, Supplementary figs. 1,2). This molecule is a sulfated metabolite of

75   cholic acid (CA), which is an abundant primary bile acid in both mice and humans. Sulfation of

76   bile acids predominantly occurs in the liver[14]. Consistent with this observation, we found increased

77   levels of CA7S in the liver of SG mice (Fig. 2d). While previous studies observed an increase in

78   the total circulating serum bile acid concentration in patients post-bariatric surgery[8], we did not

79   note a difference in total gut bile acid levels as measured in cecal contents of post-SG compared

80   to post-sham mice (Fig. 2b). Notably, CA7S was the only bile acid detected whose levels were

81   significantly higher in SG mouse cecal contents and livers (Supplementary figs. 3, 4).

82

83   To determine whether CA7S concentrations were also higher in humans after surgery, we

84   quantified bile acids in stool from patients who had undergone SG. Remarkably, even though total

85   fecal bile acid levels were decreased in patients post-SG compared to their pre-surgery levels,

86   fecal CA7S levels were significantly increased (Fig. 2e, Supplementary fig. 5). To our knowledge,

87   this is the first report of a specific bile acid metabolite that is significantly increased following SG

88   in both mice and human subjects. Similar to DIO mouse cecal contents, there was no significant

89   difference in total bile acid concentration in feces before or after SG in these patients (Fig. 2e,

90   Supplementary fig. 5).

91

92   **CA7S activates TGR5 and induces GLP-1 secretion in vitro**

93   We next sought to determine whether CA7S can activate TGR5 and thereby induce GLP-1

94   secretion from L cells. Previous work has shown that sulfation of both natural bile acids and

4

95   synthetic analogs significantly alters the TGR5 agonistic activity of these compounds[15]. We

96   therefore hypothesized that CA7S might possess altered TGR5 agonism compared to CA. While

97   sulfation at C3 abolishes the TGR5 agonist activity of lithocholic acid (EC_{50} values of 0.58 μM and

98   >100 μM, respectively), replacement of the C24-carboxylic acid with a C24-sulfate lowers the

99   EC_{50} of CA, chenodeoxycholic acid, and ursodeoxycholic acid by an order of magnitude in each

100 case[15]. Based on these results, we hypothesized that the C7-sulfated version of CA, CA7S, might

101 possess significantly different TGR5 agonistic activities than CA, which is a weak agonist of TGR5

102 (reported EC_{50} value of 13.6 uM)[15]. We examined the activation of human TGR5 in human

103 embryonic kidney cells (HEK293T) by CA7S, CA, or tauro-deoxycholic acid (TDCA), which is a

104 naturally occurring bile acid and potent TGR5 agonist[16]. We found that CA7S activated human

105 TGR5 in a dose-dependent manner and to a similar extent as TDCA. CA7S also displayed a lower

106 EC_{50} (0.17 μM) than CA (12.22 μM) (Fig. 2f).

107

108 TDCA is currently one of the most potent, naturally occurring GLP-1 secretagogues known[16]. We

109 observed that CA7S induced GLP-1 secretion in human intestinal L cells (NCI-H716) to a similar

110 degree as TDCA in a dose-dependent manner, while CA had no effect on GLP-1 secretion (Fig.

111 2g and Supplementary fig. 6a). CA7S extracted and purified directly from cecal contents of SG

112 mice also induced GLP-1 secretion in vitro (Fig. 2h). Furthermore, siRNA-mediated knockdown

113 of TGR5 abolished both CA7S- and TDCA-mediated secretion of GLP-1 (Fig. 2g, Supplementary

114 fig. 6a,b). This result indicates that induction of GLP-1 secretion by CA7S requires TGR5. TGR5

115 agonism also results in elevated intracellular calcium levels[17]. Consistent with this previous

116 finding, we observed a dose-dependent increase in calcium levels in NCI-H716 cells treated with

117 CA7S (Supplementary fig. 6c). Taken together, our results demonstrate that CA7S, a naturally

118 occurring bile acid metabolite, is a potent TGR5 agonist and GLP-1 secretagogue.

119

120   **Acute enteral CA7S administration induces GLP-1 expression and reduces blood glucose**

121   **in vivo**

122   We next evaluated the acute anti-diabetic effects of CA7S in vivo. DIO mice were treated with

123   either CA7S or PBS via duodenal and rectal catheters (Fig. 3a). Administration of 1 mg of CA7S

124   resulted in an average of 2500 pmol/mg wet mass of CA7S in cecal contents, a concentration

125   similar to observed post-SG levels (Fig. 2b, 3b, Table 1). Consistent with our in vitro studies,

126   CA7S-treated mice displayed increased systemic GLP-1 levels compared to PBS-treated mice

127   within 15 minutes (Fig. 3c). Moreover, CA7S-treated mice exhibited reduced blood glucose levels

128   and increased insulin levels compared to PBS-treated mice (Fig. 3d,e, Supplementary fig. 6d).

129   GLP-1-producing enteroendocrine L cells are enriched in the distal compared to the proximal

130   gut[18,19]. Consistent with this finding, we observed that TGR5 expression was increased in the

131   colon, but not the terminal ileum, of CA7S-treated mice (Fig. 3f). These results suggest that in an

132   acute setting, distal action of CA7S in the GI tract induces systemic glucose clearance and thus

133   ameliorates hyperglycemia.

134

135   **Oral CA7S administration increases glucose tolerance in vivo**

136   To further study the anti-diabetic effects of CA7S, DIO mice were orally gavaged with CA7S at a

137   dose of 100 mg/kg (Fig. 4a). Analysis of cecal contents 5 hours post-gavage showed an

138   accumulation of 15,000 picomol/mg wet mass of CA7S (mean value, Fig. 4b), a concentration

139   that is within an order of magnitude of the mean amount measured in post-SG mice. These data

140   indicate that we had administered a physiologically relevant concentration of this metabolite.

141   Systemic levels of GLP-1 were increased in CA7S-gavaged mice compared to PBS-treated mice

142   5 hours post-treatment (Fig. 4c). This result is consistent with the findings from enteral

143   administration and demonstrates that oral CA7S treatment can increase circulating GLP-1 for

144   several hours.

145

146   We then determined the effect of CA7S on glucose tolerance over time using an oral glucose

147   tolerance test (OGTT). DIO mice were gavaged with CA7S (100 mg/kg) or PBS and then

148   administered an oral glucose bolus 3 hours later. CA7S treatment resulted in an increased rate

149   of blood glucose clearance (Fig. 4d). Moreover, the total and incremental areas under the glucose

150   versus time curves (AUC and iAUC) were significantly decreased in CA7S- compared to vehicle-

151   treated mice (Fig. 4e). These results demonstrate that CA7S increases blood glucose clearance

152   following oral glucose challenge, a clinically relevant test used in the diagnosis of diabetes.

153

154   **Anti-diabetic effects of CA7S are largely dependent on GLP-1**

155   Because CA7S is a potent inducer of GLP-1 secretion, we sought to determine if the acute anti-

156   diabetic effects of CA7S are dependent on GLP-1. To investigate this question, we performed

157   lentiviral shRNA-mediated knockdown of the GLP-1 receptor (GLP-1R) in vivo. DIO mice were

158   injected intraperitoneally with 5×10^5 shRNA lentiviral particles targeting GLP-1R. At day 3 post-

159   injection, expression of GLP-1R in the small intestine, heart, and stomach was significantly

160   reduced, and importantly, the expression of GLP-1R was undetectable in the pancreas

161   (Supplementary fig. 7a). Mice were then gavaged with CA7S (100 mg/kg) or PBS and subjected

162   to an OGTT 3 hours post-gavage. We observed that while the glycemic curve and AUCs for the

163   CA7S-treated animals were lower than those of the PBS-treated mice, there were no longer

164   significant differences in these metrics in the absence of GLP-1R. These data suggest that in an

165   acute setting, the blood glucose clearing-effects of CA7S are largely dependent on the action of

166   GLP-1 (Fig. 4f,g).

167

168   **CA7S is gut-restricted, non-toxic, and does not induce gallbladder filling**

169   While high concentrations of CA7S were observed in the intestine, this metabolite was

170   undetectable in both circulating and portal venous blood from SG and sham-operated mice (Table

171   1). This result suggests that CA7S is neither recycled via enterohepatic circulation nor absorbed

7

172   into systemic circulation. In contrast, the known endogenous TGR5 agonists TDCA and DCA are

173   found in systemic circulation in mice[9]. Introduction of CA7S via enteral administration or oral

174   gavage resulted in only minor amounts in circulating and portal venous blood (Table 1). Our

175   findings are consistent with previous observations that sulfated bile acids, in particular 7α-sulfated

176   bile acids, are poorly absorbed in the intestine[14].

177

178   Notably, while synthetic TGR5 agonists ameliorate diabetic phenotypes[20], their use as

179   therapeutics is hampered by significant side effects resulting from their absorption into circulation

180   [20,21]. In particular, systemically absorbed TGR5 agonists reduce bile secretion and induce

181   gallbladder filling, conditions that cause bile stasis[10,21]. We did not observe any change in

182   gallbladder weight in DIO mice 5 hours after oral gavage of CA7S compared to PBS control

183   treatment (Fig. 4h). This result suggests that, in an acute setting, CA7S does not display one of

184   the major side-effects of non-gut-restricted TGR5 agonists. Finally, CA7S does not affect the

185   viability of Caco-2 cells at concentrations up to 15 mM (Fig. 4i), indicating that this metabolite is

186   not toxic to human intestinal cells at physiologically relevant concentrations.

187

188   **Discussion**

189   By quantifying changes in individual bile acids, we found that the sulfated metabolite CA7S is

190   increased in both the mouse GI tract and human feces following SG. We then found that CA7S is

191   a potent TGR5 agonist that induces the secretion of the incretin hormone, GLP-1 from

192   enteroendocrine L cells both in vitro and in vivo. In acute settings, we observed that CA7S exhibits

193   anti-diabetic effects, including decreasing blood glucose levels and increasing glucose tolerance

194   in insulin-resistant mice. Unlike known endogenous TGR5 agonists, CA7S is not absorbed into

195   portal or systemic circulation. CA7S had previously been regarded as a metabolic waste product

196   produced by the liver – a sulfated form of cholic acid that was tagged for excretion in feces[14]. To

197   our knowledge, no role for CA7S as a ligand for a GPCR or NhR has been reported. Taken

8

198   together, our data indicate that CA7S is a signaling molecule that binds to TGR5 exclusively in

199   the gut and thereby increases systemic levels of GLP-1.

200

201   Owing to the significant off-target effects caused by TGR5 agonists absorbed into circulation, it

202   has been suggested that an improved TGR5-based therapeutic for T2D would specifically activate

203   intestinal TGR5[21]. This GPCR is expressed both apically and basolaterally on L cells[16]. TDCA has

204   been shown to activate TGR5 and induce GLP-1 secretion when applied to L cells from both

205   apical and basolateral directions [16]. These findings suggest that development of a gut-restricted

206   TGR5 agonist could be effective in the treatment of T2D. In the setting of acute administration,

207   we found that CA7S does not induce gallbladder filling as has been reported for synthetic TGR5

208   agonists that enter circulating blood. Furthermore, CA7S is not toxic to human intestinal cells and

209   is stable at physiological pHs (Supplementary fig. 7b). Additional studies are required to assess

210   the long-term effects of CA7S on glucose tolerance and insulin sensitivity in vivo. Nonetheless,

211   as a result of its beneficial acute metabolic effects, gut restriction, and low toxicity, CA7S could

212   be a candidate for the development of a T2D therapeutic.

213

214   The role that CA7S plays in the metabolic changes observed post-SG remains unknown. Due to

215   the redundancy of sulfotransferases (SULTs), the enzymes responsible for CA7S synthesis in the

216   the mouse liver[22], knock-down of endogenous CA7S levels may be a challenging endeavor. If this

217   obstacle could be overcome, performing SG on CA7S-depleted mice would help to reveal the

218   contribution of this molecule to the metabolic effects of the surgery.

219

220   More broadly, prior to this work, there were no known individual metabolites whose levels were

221   altered by bariatric surgery that could increase blood glucose clearance. Through the

222   identification and study of CA7S, we have uncovered a metabolite that, while restricted to the GI

223   tract, can improve global glucose regulation.

224 **Online Methods**

225 **Animals**. Diet induced obese, male, C57Bl/6J mice were purchased from Jackson Laboratory

226 (Bar Harbor, ME) at 11-16 weeks of age. They were housed under standard conditions in a

227 climate-controlled environment with 12 hour light and dark cycles and reared on a high fat diet

228 (HFD, 60% Kcal fat; RD12492; Research Diets, NJ). They were allowed to acclimate for at least

229 1 week prior to undergoing any procedures. All animals were cared for according to guidelines

230 set forth by the American Association for Laboratory Animal Science. All procedures were

231 approved by the Institutional Animal Care and Use Committee.

232

233 **Sleeve gastrectomy (SG) and sham procedures**. 11-week-old DIO mice were purchased and

234 housed as described above. Mice were weight-matched into two groups and either underwent SG

235 or Sham operation. SG was performed through a 1.5 cm midline laparotomy under isoflurane

236 anesthesia. The stomach was gently dissected free from its surrounding attachments, the vessels

237 between the spleen and stomach (short gastric vessels) were divided, and a tubular stomach was

238 created by removing 80% of the glandular and 100% of the non-glandular stomach with a linear-

239 cutting surgical stapler. Sham operation consisted of a similar laparotomy, stomach dissection,

240 ligation of short gastric vessels, and manipulation of the stomach along the staple line equivalent.

241 Mice were then individually housed thereafter to allow for monitoring of food intake, weight, and

242 behavior. SG and Sham mice were maintained on Recovery Gel Diet (Clear H_2O, Westbrook,

243 ME) from 1 day prior through 6 days after surgery and then were restarted on HFD on the morning

244 of post-operative day (POD) 7. Mice were sacrificed 5-7 weeks post-surgery.

245

246 **Functional glucose testing**. After a 4 hour fast (8 am to noon), intraperitoneal glucose tolerance

247 testing (IPGTT) and insulin tolerance testing (ITT) were performed at post-operative week 4 and

248 5, respectively. During IPGTT, mice received 2 mg/g of intraperitoneal D-Glucose (Sigma-Aldrich,

249 St. Louis, MO) and serum glucose levels were measured from the tail vein at 15, 30, 60, and 120

10

250   min with a OneTouch Glucometer (Life technologies, San Diego, CA). ITT was performed by

251   intraperitoneal instillation of 0.6u/kg of regular human insulin (Eli Lily and Company, Indianapolis,

252   IN) and measurement of serum glucose levels at 15, 30, and 60 min. Baseline glucose was

253   measured for each set prior to medication administration.

254

255   **Body weight and food intake measurements**. Mice were individually housed and weighed daily

256   for the first post-operative week and then twice weekly until sacrifice. Food intake was measured

257   twice weekly and daily food intake was calculated by averaging the grams eaten per day over the

258   preceding days. Note that food intake measurements were started on POD 10 as animals were

259   transitioned from Gel Diet to high fat diet on the morning of POD 7.

260

261   **Bile acid analysis**. Bile acid analyses were performed using a previously reported method[23].

262   <u>Reagents</u>. Stock solutions of all bile acids were prepared by dissolving the compounds in

263   molecular biology grade DMSO (VWR International, Radnor, PA). These solutions were used to

264   establish standard curves. CA7S was purchased from (Caymen Chemicals, Ann Arbor, MI. Cat.

265   No. 9002532). Glyocholic acid (GCA) (Sigma) was used as the internal standard for

266   measurements in mouse tissues. HPLC grade solvents were used for preparing and running

267   UPLC-MS samples.

268   <u>Extraction</u>. Cecal, liver, and human fecal samples (approximately 50 mg each) and mouse portal

269   veins were pre-weighed in lysis tubes containing ceramic beads (Precellys lysing kit tough micro-

270   organism lysing VK05 tubes for cecal, fecal samples, and portal veins; tissue homogenizing

271   CKMix tubes for liver samples; Bertin technologies, Montigny-le-Bretonneux, France). 400µL of

272   methanol containing 10 µM internal standard (GCA) was added and the tubes were homogenized

273   in a MagNA Lyser (6000 speed for 90 s*2, 7000 speed for 60 s). 50 µl of mouse serum was

274   collected in Eppendorf tubes, followed by addition of 50 µL of methanol containing 10 µM internal

275   standard (GCA). After vortexing for 1 min, the sample was cooled to −20 °C for 20 min. All

11

276   methanol-extracted tissue samples were centrifuged at 4 °C for 30 min at 15,000 rpm. The

277   supernatant was diluted 1:1 in 50% methanol/water and centrifuged again at 4 °C for 30 min at

278   15000 rpm. The supernatant was transferred into mass spec vials and injected into the UPLC-

279   MS.

280   UPLC-MS analysis. Samples were injected onto a Phenomenex 1.7 µm, C18 100 Å, 100 × 21

281   mm LC column at room temperature and eluted using a 30 min gradient of 75% A to 100% B

282   (A = water + 0.05% formic acid; B = acetone + 0.05% formic acid) at a flow rate of 0.350 mL/min.

283   Samples were analyzed using an Agilent Technologies 1290 Infinity II UPLC system coupled

284   online to an Agilent Technologies 6120 Quadrupole LC/MS spectrometer in negative electrospray

285   mode with a scan range of 350–550 m/z (MSD settings: fragmentor - 250, gain - 3.00, threshold

286   - 150, Step size - 0.10, speed (u/sec) - 743). Capillary voltage was 4500 V, drying gas temperature

287   was 300°C, and drying gas flow was 3 L/min. Analytes were identified according to their mass

288   and retention time. For quantification of the analytes, standard curves were obtained using known

289   bile acids, and then each analyte was quantified based on the standard curve and normalized

290   based on the internal standard. The limits of detection for individual bile acids were determined

291   using commercially available standards solubilized in 1:1 MeOH/water and are as follows: CA7S,

292   0.05 picomol/µL; α/βMCA, 0.03 picomol/µL; Tα/βMCA, 0.01 picomol/µL; CA, 0.04 picomol/µL;

293   TCA, 0.01 picomol/µL; UDCA, 0.04 picomol/µL; TUDCA, 0.01; CDCA, 0.04 picmol/µL; TCDCA,

294   0.01 picomol/µL; LCA, 0.03 picomol/µL; isoLCA, 0.07 picomol/µL; 3-oxo-LCA, 0.05 picomol/µL;

295   DCA, 0.04 picomol/µL; 3-oxo-CA, 0.04 picomol/µL; 3-oxo-CDCA, 0.4 picomol/µL; 7-oxo-CDCA,

296   0.03 picomol/µL. Note that CA7S and cholic acid-3-sulfate can be distinguished based on

297   retention time using this UPLC-MS method.

298   Purification of CA7S. Extracted cecal contents from 11 SG mice (same shown in Fig. 1) were

299   pooled to provide sufficient material for purification. Pooled extract was purified via MS-guided

300   HPLC of m/z 487 using a Luna RP C18 semi-preparative column and water and acetonitrile with

301   0.1% formic acid as an additive.

12

302   NMR spectroscopy. CA7S and purified *m/z* 487 (<1 mg) were dissolved in 250 μL DMSO-d6.

303   Nuclear magnetic resonance (NMR) spectra were acquired on a Varian INOVA 500 MHz and are

304   referenced internally according to residual solvent signals (DMSO to 2.50, HOD to 3.33).

305

306   **Cell culture**. NCI-H716 cells and Caco-2 cells were obtained from American Type Culture

307   Collection (Manassas, VA). HEK-293T cells were a kind gift from the Blacklow lab (BCMP, HMS).

308   Caco-2 and HEK-293T cells were maintained in Minimum Essential Medium (MEM) with

309   GlutaMAX and Earle's Salts (Gibco, Life Technologies, UK). NCI-H716 cells were maintained in

310   RPMI 1640 with L-glutamine (GenClone, San Diego, CA). All cell culture media were

311   supplemented with 10% fetal bovine serum (FBS), 100 units/ml penicillin, and 100 μg/ml

312   streptomycin (GenClone). Cells were grown in FBS- and antibiotic-supplemented 'complete'

313   media at 37 °C in an atmosphere of 5% CO_2.

314

315   **In vitro bile acid treatments**. NCI-H716 cells were seeded in cell culture plates coated with

316   Matrigel (Corning, NY. Cat. No. 356234) diluted in Hank's Balanced Salt Solution (HBSS, Gibco)

317   according to manufacturer's instructions. The cells were allowed to grow for 2 days in complete

318   RPMI media. On the day of the treatment, cells were rinsed gently with low serum (0.5% FBS)

319   RPMI 1640 medium without antibiotics. Bile acids cholic acid-7-sulfate (CA7S), cholic acid (CA)

320   (Sigma) and taurodeoxycholic acid (TDCA) (Sigma) were diluted in dimethyl sulfoxide (DMSO,

321   VWR International) and added to cells in the low serum media (0.5% FBS, RPMI 1640) without

322   antibiotics. The concentration of DMSO was kept constant throughout the treatments and used

323   as a negative control. Cells were incubated at 37°C in an atmosphere of 5% CO_2 for 2 hours. After

324   the incubation period, cell culture media was collected in Eppendorf tubes containing 1%

325   trifluoroacetic acid (TFA, Sigma) in sterile purified water (GenClone) to make a final TFA

326   concentration of 0.1% and frozen at -80 °C for further GLP-1 measurements. Cells on cell culture

327   plates were placed on ice and gently washed with PBS (GenClone). Cells used for GLP-1

13

328   measurements were treated with ice-cold cell lysis solution of 1% TFA, 1N hydrochloric acid, 5%

329   formic acid, and 1% NaCl (all from Sigma), scraped off of the Matrigel coating, and collected in

330   lysing tubes with ceramic beads (Precellys lysing kit tough micro-organism lysing VK05 tubes).

331   For calcium measurements, PBS was added to cells, and were collected in lysing tubes containing

332   ceramic beads (Precellys lysing kit tough micro-organism lysing VK05 tubes). Cells

333   were thereafter lysed in a MagNA Lyser and stored at -80 °C for further analysis. Cells used for

334   RNA extraction were treated with TRIzol (Ambion, Life Technologies, Thermo Fisher Scientific,

335   Waltham, MA) and stored at -80 °C for further analysis.

336

337   **GLP-1 and Insulin measurements**. Total GLP-1 peptide measurements were performed using

338   the GLP-1 EIA Kit (Sigma, Cat. No. RAB0201) and total insulin levels were measured using the

339   Mouse Ins1/Insulin-1 ELISA kit (Sigma, Cat. No. RAB0817) according to manufacturer's

340   instructions. Mouse serum samples, NCI-H716 cell lysates, and cell culture media samples were

341   stored at -80 °C and thawed on ice prior to performance ELISA assay. 20 µl of mouse serum

342   samples were used directly in the GLP-1 ELISA assay, while 50 µl of mouse serum samples were

343   used directly in the Insulin ELISA assay. Cell culture media were centrifuged at 12000 rpm, and

344   the supernatant was directly used in the GLP-1 ELISA assay. Cell lysates were subjected to

345   peptide purification using Sep Pak C18 Classic columns (Waters Corporation, Milford, MA). The

346   column was pretreated with a solution of 0.1% TFA in 80% isopropyl alcohol (EMD Millipore) and

347   equilibrated with 0.1% TFA in water. Cell lysates were loaded onto the column and washed with

348   0.1% TFA in 80% isopropyl alcohol. The peptides were eluted in 0.1% TFA in water. The eluate

349   was concentrated by drying under vacuum and resuspended in 0.1% TFA in water. Water was

350   used as 'blank' reading for serum GLP-1 ELISA, while 0.1% TFA in water was used as 'blank' for

351   cell culture media and purified cell lysate ELISAs. Excess samples were stored at -80°C for later

352   analyses. Total GLP-1 amounts in the cell culture media (secreted) and cell lysates were

14

353   calculated using a standard curve provided in the EIA kit. Percentage GLP-1 secretion was

354   calculated as follows:

355   % GLP-1 secretion = total GLP-1 secreted (media) / (total GLP-1 secreted (media) + total GLP-1

356   in cell lysates) * 100. Relative GLP-1 secretion was calculated compared to DMSO control.

357

358   **Plasmids and transient transfections**. Human TGR5 was cloned using cDNA from human

359   Caco-2 cells as template and a forward primer with an *EcoRI* restriction-site (5'-

360   CGGAATTCGCACTTGGTCCTTGTGCTCT-3') and a reverse primer with a *XhoI*-site (5'-

361   GTCTCGAGTTAGTTCAAGTCCAGGTCGA-3'). The PCR product was cloned into the pCDNA

362   3.1+ plasmid (Promega Corporation, Madison, WI) and transfected at a concentration of 0.4 µg/ml

363   of media. For luciferase reporter assays for TGR5 activation, the pGL4.29[luc2P/CRE/Hygro]

364   plasmid (Promega Corporation), and the pGL4.74[hRluc/CMV] plasmid (Promega Corporation)

365   were used at concentration of 2 µg/ml and 0.05 µg/ml of media respectively. All plasmids were

366   transfected using Opti-MEM (Gibco) and Lipofectamine 2000 (Invitrogen, Life Technologies,

367   Grand Island, NY, USA) according to manufacturer's instructions. Plasmid transfection were

368   performed in antibiotic-free media (MEM for HEK293T and RPMI for Matrigel-attached NCI-H716

369   cells) with 10% FBS. After overnight incubation, bile acids were added in complete media and

370   incubated overnight. Cells were harvested the next day for luciferase assay. TGR5 siRNA (Santa

371   Cruz Biotechnology, Dallas, TX) and negative siRNA (Ambion) transfection was performed using

372   Opti-MEM and Lipofectamine 2000 according to manufacturer's instructions. After siRNA

373   transfection, cells were incubated in antibiotic- and serum-free media (RPMI for Matrigel-attached

374   NCI-H716 cells) for 24 hours. The next day, the media was replaced by complete media and

375   incubated overnight. Bile acids were added 48 hours post-siRNA transfection in complete media

376   and incubated overnight. Cells were harvested the next day for luciferase assay or RNA

377   extraction.

378

15

379 **Luciferase reporter assay**. Luminescence was measured using the Dual-Luciferase Reporter

380 Assay System (Promega Corporation) according to manufacturer's instructions. Cells were

381 washed gently with PBS and lysed in PLB from the kit. Matrigel-attached cells were scraped in

382 PLB. Luminescence was measured using the SpectraMax M5 plate reader (Molecular Devices,

383 San Jose, CA) at the ICCB-Longwood Screening Facility at Harvard Medical School.

384 Luminescence was normalized to *Renilla* luciferase activity and percentage relative luminescence

385 was calculated compared to DMSO control.

386

387 **Calcium measurement**. CA7S-treated NCI-H716 cells collected in PBS were used to measure

388 intracellular calcium using the Calcium Assay Kit (Fluorometric) (Abcam, UK). Cell lysates were

389 centrifuged at 12000 rpm, and the supernatant was directly used in the calcium assay according

390 to manufacturer's instructions. Fluorescence was measured using the SpectraMax M5 plate

391 reader (Molecular Devices, San Jose, CA) at the ICCB-Longwood Screening Facility at HMS.

392 Percentage relative fluorescence was calculated compared to DMSO control.

393

394 **Cell viability assay**. Caco-2 cells were treated with CA7S diluted in DMSO in complete MEM

395 media. The concentration of DMSO was kept constant and used as a negative control. Cells were

396 incubated with CA7S overnight at 37 °C in an atmosphere of 5% CO_2. The next day, cells were

397 treated with 0.25% trypsin in HBSS (GenClone) for 10 min at 37°C. Cell viability was measured

398 in Countess II automated cell counter (Invitrogen). Percentage relative viability was calculated

399 compared to DMSO control.

400

401 **pH stability test**. Stability of CA7S in physiological pH's was determined using the Waters pH

402 stability test. Briefly, buffers of pH 1 (0.1M HCl), pH7.4 (PBS) and pH 9 (a 10 mM solution of

403 ammonium formate adjusted to pH 9 with ammonium hydroxide) (all from Sigma) were prepared.

404 CA7S was incubated in the pH buffers overnight at 37 °C with gentle shaking (50 rpm). The next

16

405   day, the CA7S solution was diluted in methanol, transferred into mass spec vials and injected into

406   the UPLC-MS.

407

408   **RNA extraction and qPCR**. Cells frozen in TRIzol (Ambion) were collected in RNase-free

409   Eppendorf tubes and vortexed for 30 seconds. Tissues were collected in Precellys tubes with

410   ceramic beads and TRIzol, followed by homogenization in a MagNA Lyser (Roche, Switzerland).

411   Tubes were kept on ice whenever possible. Chloroform was added (200μl chloroform/1ml TRIzol)

412   and vortexed for 30 seconds. Tubes were centrifuged at 12,000 rpm for 15 min at 4 ºC. The clear

413   top layer was transferred to new RNase-free Eppendorf tubes containing 2-propanol and inverted

414   to mix (500μl 2-propanol/1ml TRIzol). Tubes were centrifuged at 12,000 rpm for 10 min at 4 ºC.

415   The pellet was washed with 70% EtOH and centrifuged at 14,000rpm for 5 minutes at 4 ºC. The

416   RNA pellet was air-dried and resuspended in RNase-free H_2O (GenClone). cDNA synthesis was

417   performed using the High Capacity cDNA Reverse Transcription Kit (Applied Biosystems,

418   Invitrogen, Foster City, CA). qPCR was performed using the Lightcycler 480 SYBR Green I Mater

419   (Roche, Switzerland) in a 384-well format using a LightCycler 480 System (Roche) at the ICCB-

420   Longwood Screening Facility at Harvard Medical School. Cq values above 45 were considered

421   as not detected (n.d.). The $2^{-\Delta\Delta Ct}$ method was used to calculate the relative change in gene

422   expression. Human *TGR5* gene expression were normalized to the human *HPRT1* (*HGPRT*).

423   Mouse *GLP-1R* gene expression was normalized to 18S. Primer sequences were:

424   human *TGR5*: Forward: 5'-CCTAGGAAGTGCCAGTGCAG-3', Reverse: 5'-

425   CTTGGGTGGTAGGCAATGCT-3'; human *HGPRT*: Forward: 5'-

426   CCTGGCGTCGTGATTAGTGA-3', Reverse: 5' CGAGCAAGACGTTCAGTCCT-3'; mouse *GLP-

427   1R*: Forward: 5'- AGGGCTTGATGGTGGCTATC -3', Reverse: 5'-

428   GGACACTTGAGGGGCTTCAT -3'; mouse 18S: Forward: 5'ATTGGAGCTGGAATTACCGC-3',

429   Reverse: 5'CGGCTACCACATCCAAGGAA-3'.

430

17

431 **In vivo enteral treatment with CA7S**. 13-week-old male C57Bl/6J mice were purchased,

432 acclimated, and housed as above. They were weight matched into two groups (p=0.88). After an

433 overnight fast (17:00 to 0800), mice received either CA7S or PBS via direct duodenal and rectal

434 administration. The optimal, physiologic dose of CA7S was extrapolated from the average pmol

435 concentration of CA7S found in cecal samples from SG animals (average of 3000 pmol/mg of

436 stool with 500 mg of stool per animal corresponds to 0.75 mg of CA7S per cecum).

437 Under isoflurane general anesthesia, 0.25 mg and 0.75 mg of CA7S in PBS (pH 7.2) was

438 delivered by slow infusion (5 min) antegrade into the duodenum and retrograde into the rectum,

439 respectively. The total volume of instillation was 2 mL (0.5 mg CA7S/mL). Control animals

440 received similar volumes of PBS alone. 15 min post infusion, serum glucose was measured via

441 tail vein followed by whole blood collection via cardiac puncture into K+EDTA tubes containing

442 DPPIV inhibitor (Merck Millipore, Billerica, MA), Perfabloc (Sigma), and apoprotinin (Sigma).

443 Organs were harvested for analysis. In order to account for changes in fasting times and hormonal

444 diurnal rhythms, this experiment was carried out on four consecutive days such that only four

445 mice were tested per day.

446

447 **In vivo CA7S gavage**. 16-week-old DIO mice were purchased and housed as described above.

448 Mice were gavaged orally with 100 mg/kg CA7S from 20 mg/mL solution, or equivalent volume of

449 PBS using 20G x 38mm gavage needle. 5 hours after CA7S/PBS administration, whole blood and

450 intestinal segments were collected.

451

452 **In vivo CA7S and OGTT**. Age matched, DIO mice were kept on HFD and their blood glucose

453 levels were monitored until average fasting glucose levels were >160 mg/dL. Animals were fasted

454 for 4 hours on the day of the experiment. Mice were matched into two groups based on fasting

455 glucose levels and received either 100 mg/kg CA7S from a 20 mg/ml solution or an equivalent

456 volume of PBS by oral gavage. Three hours later, an OGTT was performed using an oral gavage

18

457   of 2 mg/g oral D-glucose (Sigma-Aldrich, St. Louis, MO). Blood glucose levels were measured at

458   baseline and at minutes 15, 30, 60 and 120 with a OneTouch glucometer.

459

460   **Lentiviral IP injection**. GLP-1R shRNA-containing lentiviral particles (LVP) were purchased from

461   the MISSION TRC library (Sigma-Aldrich, St. Louis, MO). LVPs containing a mixture of three GLP-

462   1R shRNA plasmid clones (TRCN0000004629, TRCN0000004630, and TRCN0000004633) were

463   purchased, stored at -80 ºC, and thawed on ice before use. DIO mice were maintained on a HFD

464   until average fasting glucose >160 mg/dL in a BL2 facility. Under sterile conditions, mice were

465   injected intraperitoneally with 0.2 ml of 5×10^5 GLP-1R shRNA LVPs with a 27G needle[24,25]. 72

466   hours after LVP injection, mice underwent CA7S/PBS gavage followed by OGTT as above. After

467   the OGTT was completed, mice were sacrificed and their tissues were harvested. GLP-1R knock-

468   down efficiency was measured in tissues by qPCR as described above.

469

470   **Human stool collection**. After obtaining institutional review board approval, we prospectively

471   collected stool specimen from obese human subjects undergoing SG. Pre-operative stool

472   specimen were collected on the day of surgery and post-operative stool specimen were obtained

473   from post-operative day 14 to 99 (mode 15 days; median 36 days). Specimens were snap frozen

474   in liquid nitrogen and stored at -80 ºC until bile acid analysis was performed (as above).

475

476

Author contributions

A.S.D., E.G.S., S.N.C., and D.A.H. conceived the project and designed the experiments. S.N.C. performed the cell culture experiments, bile acid profiling, and transcriptional analyses and hormone quantifications on mouse tissues and blood. D.A.H. performed the surgeries and the enteral administration in vivo experiments. H.A. and R.S. performed the gavages, OGTTs, and the lentiviral injection experiments. M.T.H. performed NMR analyses. A.H.V. collected and provided the human samples. S.N.C., D.A.H., E.G.S., and A.S.D. wrote the manuscript. A.T. provided feedback and reviewed the manuscript. All authors edited and contributed to the critical review of the manuscript.

Competing interests

CA7S is a subject of provisional patents held by HMS and BWH on which S.N.C., D.A.H., E.G.S., and A.S.D. are inventors. A.S.D. is a consultant for Kintai Therapeutics and HP Hood. E.G.S. was previously on the scientific advisory board of Kitotech, Inc.

Data availability statement

All data generated or analyzed during this study are included in this article and its supplementary

information files. In addition, numerical values for levels of individual bile acids shown as individual

data points in Figure 2 and Supplementary Figures 3, 4, and 5 are available from the

corresponding author upon reasonable request.

Code availability statement

No custom code or mathematical algorithms were used in this study.

References

1. Batterham, R. L. & Cummings, D. E. Mechanisms of Diabetes Improvement Following Bariatric/Metabolic Surgery. *Diabetes Care* **39,** 893–901 (2016).
2. Gloy, V. L. *et al.* Bariatric surgery versus non-surgical treatment for obesity: a systematic review and meta-analysis of randomised controlled trials. *BMJ* **347,** f5934–f5934 (2013).
3. Abbasi, J. Unveiling the 'Magic' of Diabetes Remission After Weight-Loss Surgery. *JAMA* **317,** 571–574 (2017).
4. Kaska, L., Sledzinski, T., Chomiczewska, A., Dettlaff-Pokora, A. & Swierczynski, J. Improved glucose metabolism following bariatric surgery is associated with increased circulating bile acid concentrations and remodeling of the gut microbiome. *World J. Gastroenterol.* **22,** 8698–8719 (2016).
5. Fiorucci, S. & Distrutti, E. Bile Acid-Activated Receptors, Intestinal Microbiota, and the Treatment of Metabolic Disorders. *Trends Mol Med* **21,** 702–714 (2015).
6. McGavigan, A. K. *et al.* TGR5 contributes to glucoregulatory improvements after vertical sleeve gastrectomy in mice. *Gut* **66,** 226–234 (2017).
7. Ryan, K. K. *et al.* FXR is a molecular target for the effects of vertical sleeve gastrectomy. *Nature* **509,** 183–188 (2014).
8. Patti, M.-E. *et al.* Serum bile acids are higher in humans with prior gastric bypass: potential contribution to improved glucose and lipid metabolism. *Obesity (Silver Spring)* **17,** 1671–1677 (2009).
9. Sayin, S. I. *et al.* Gut microbiota regulates bile acid metabolism by reducing the levels of tauro-beta-muricholic acid, a naturally occurring FXR antagonist. *Cell Metab.* **17,** 225–235 (2013).
10. Duboc, H., Taché, Y. & Hofmann, A. F. The bile acid TGR5 membrane receptor: from basic research to clinical application. *Dig Liver Dis* **46,** 302–312 (2014).
11. Madsbad, S. The role of glucagon-like peptide-1 impairment in obesity and potential therapeutic implications. *Diabetes Obes Metab* **16,** 9–21 (2014).
12. Khorgami, Z. *et al.* Trends in utilization of bariatric surgery, 2010-2014: sleeve gastrectomy dominates. *Surg Obes Relat Dis* **13,** 774–778 (2017).
13. Lutz, T. A. & Bueter, M. The Use of Rat and Mouse Models in Bariatric Surgery Experiments. *Front Nutr* **3,** 25 (2016).

543   14.   Alnouti, Y. Bile Acid sulfation: a pathway of bile acid elimination and detoxification.
544   *Toxicol. Sci.* **108,** 225–246 (2009).
545   15.   Sato, H. *et al.* Novel Potent and Selective Bile Acid Derivatives as TGR5 Agonists:
546   Biological Screening, Structure−Activity Relationships, and Molecular Modeling Studies.
547   *Journal of Medicinal Chemistry* **51,** 1831–1841 (2008).
548   16.   Brighton, C. A. *et al.* Bile Acids Trigger GLP-1 Release Predominantly by Accessing
549   Basolaterally Located G Protein-Coupled Bile Acid Receptors. *Endocrinology* **156,** 3961–
550   3970 (2015).
551   17.   Kuhre, R. E. *et al.* Peptide production and secretion in GLUTag, NCI-H716, and STC-1
552   cells: a comparison to native L-cells. *Journal of Molecular Endocrinology* **56,** 201–211
553   (2016).
554   18.   Eissele, R. *et al.* Glucagon-like peptide-1 cells in the gastrointestinal tract and pancreas
555   of rat, pig and man. *Eur. J. Clin. Invest.* **22,** 283–291 (1992).
556   19.   Harach, T. *et al.* TGR5 potentiates GLP-1 secretion in response to anionic exchange
557   resins. *Sci Rep* **2,** 430 (2012).
558   20.   Hodge, R. J. & Nunez, D. J. Therapeutic potential of Takeda-G-protein-receptor-5 (TGR5)
559   agonists. Hope or hype? *Diabetes Obes Metab* **18,** 439–443 (2016).
560   21.   Cao, H. *et al.* Intestinally-targeted TGR5 agonists equipped with quaternary ammonium
561   have an improved hypoglycemic effect and reduced gallbladder filling effect. *Sci Rep* **6,**
562   28676 (2016).
563   22.   Dawson, P. A. & Setchell, K. D. R. Will the real bile acid sulfotransferase please stand
564   up? Identification of Sult2a8 as a major hepatic bile acid sulfonating enzyme in mice. *J.
565   Lipid Res.* **58,** 1033–1035 (2017).
566   23.   Yao, L. *et al.* A selective gut bacterial bile salt hydrolase alters host metabolism. *eLife* **7,**
567   675 (2018).
568   24.   Tiscornia, G., Singer, O., Ikawa, M. & Verma, I. M. A general method for gene knockdown
569   in mice by using lentiviral vectors expressing small interfering RNA. *PNAS* **100,** 1844–
570   1848 (2003).
571   25.   Blosser, W. *et al.* A method to assess target gene involvement in angiogenesis in vitro
572   and in vivo using lentiviral vectors expressing shRNA. *PLOS ONE* **9,** e96036 (2014).
573
574

575

Fig. 1

576
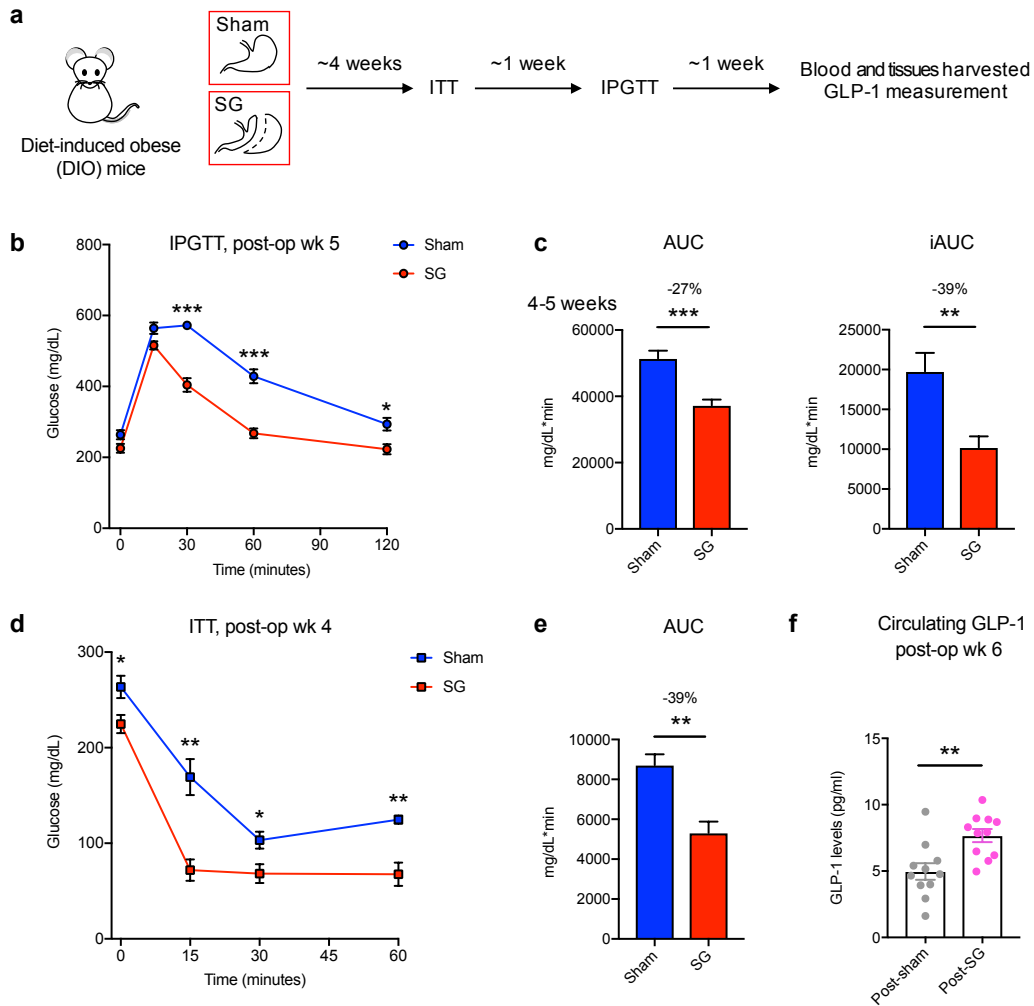
Figure 1. DIO mice display improved glucose tolerance and insulin sensitivity following SG

a, Schematic of surgical interventions and post-operative assessments. Sleeve gastrectomy (SG) or sham surgery was performed on diet-induced obese (DIO) mice, followed by an insulin tolerance test (ITT) ~4 weeks post-op and then intraperitoneal glucose tolerance test (IPGTT) ~5 weeks post-op. Blood and tissues were harvested ~6 weeks post-op. **b**, Glycemic curves during IPGTT (SG, n=7; sham, n=6, 30 min ***p=5.91x10^{-6}, 60 min ***p=4.34x10^{-5}, 120 min *p=0.012, Student's t test). **c**, Corresponding area under the blood glucose curve (AUC) and incremental area under the curve (iAUC) were reduced in SG- compared to sham-operated mice. (AUC ***p=

23

586   0.0004, iAUC **p= 0.006, Student's t test). **d**, Glycemic curves during ITT (SG, n=4; sham, n=4,

587   0 min *p=0.042, 15 min **p=0.0043, 30 min *p=0.038, 60 min **p=0.0045, Student's t test). **e**,

588   Corresponding area under the blood glucose curve (AUC) was reduced in SG- compared to

589   sham-operated mice (AUC **p= 0.005, Student's t test). **f**, GLP-1 levels were increased in mice

590   post-SG compared to post-sham (n=11 per group, **p=0.003, Welch's t test). All data are

591   presented as mean ± SEM.

592

Fig. 2
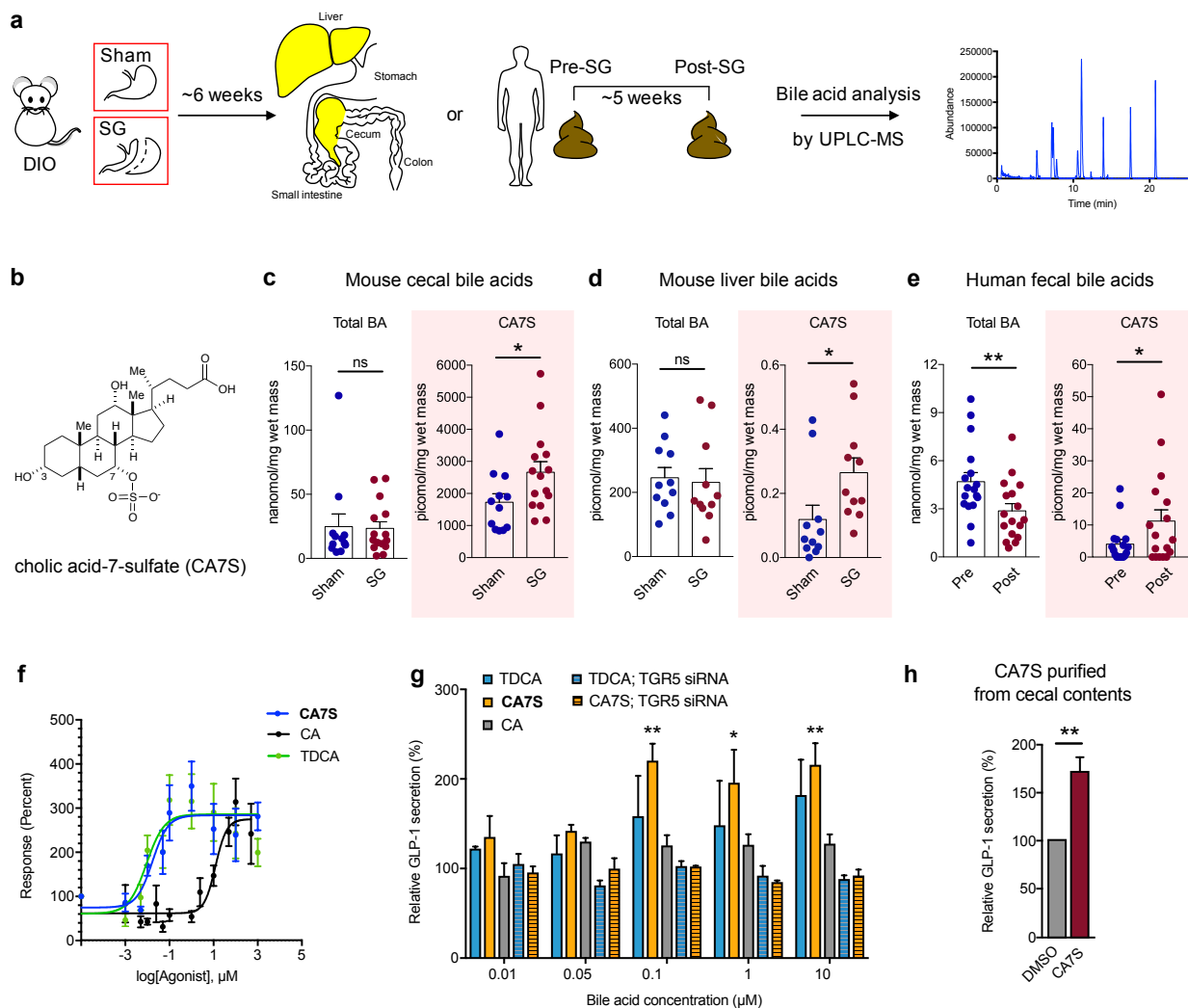
593

594   **Figure 2. Cholic acid-7-sulfate (CA7S), a bile acid metabolite increased in mice and humans**

595   **following SG, is a TGR5 agonist and induces GLP-1 secretion in vitro**

596   **a**, Schematic of sample collection followed by bile acid profiling using UPLC-MS. For mice, livers

597   and cecal contents were collected from sham or SG mice 6 weeks post-op. For humans, fecal

598   samples were collected pre-op and ~5 weeks post-op (median 36 days after surgery). **b**, Structure

599   of CA7S. **c**, CA7S was increased in cecal contents of SG mice, while total bile acid concentrations

600   did not differ between SG and sham mice (sham, n=12, SG, n=15, *p=0.037, p=0.9, ns=not

601   significant, Welch's t test). Note that 1 picomol bile acid/mg wet mass is approximately equivalent

602   to 1 µM. **d**, CA7S was increased in livers of SG mice (n=11 per group, *p=0.033, p=0.546, ns=not

603   significant, Welch's t test). **e**, CA7S in human feces was increased post-SG compared to pre-

604   surgery (n=17 patients, *p=0.015, **p=0.001, paired t test). **f**, Dose response curves for human

605   TGR5 activation in HEK293T cells overexpressing human TGR5 for CA7S, TDCA, CA ($\geq$3

606   biological replicates per condition). **g**, CA7S-induced secretion of GLP-1 in NCI-H716 cells

607   compared to both CA and the known TGR5 agonist, TDCA. siRNA-mediated knockdown of TGR5

608   abolished GLP-1 secretion ($\geq$3 biological replicates per condition, 0.1µM **p=0.008, 1µM

609   *p=0.030, 10µM **p=0.002, one-way ANOVA followed by Dunnett's multiple comparisons test).

610   **h**, CA7S (500 µM) purified from SG mouse cecal contents induced secretion of GLP-1 in NCI-

611   H716 cells compared to DMSO control (**p=0.001, Welch's t test). All data are presented as mean

612   ± SEM.

25
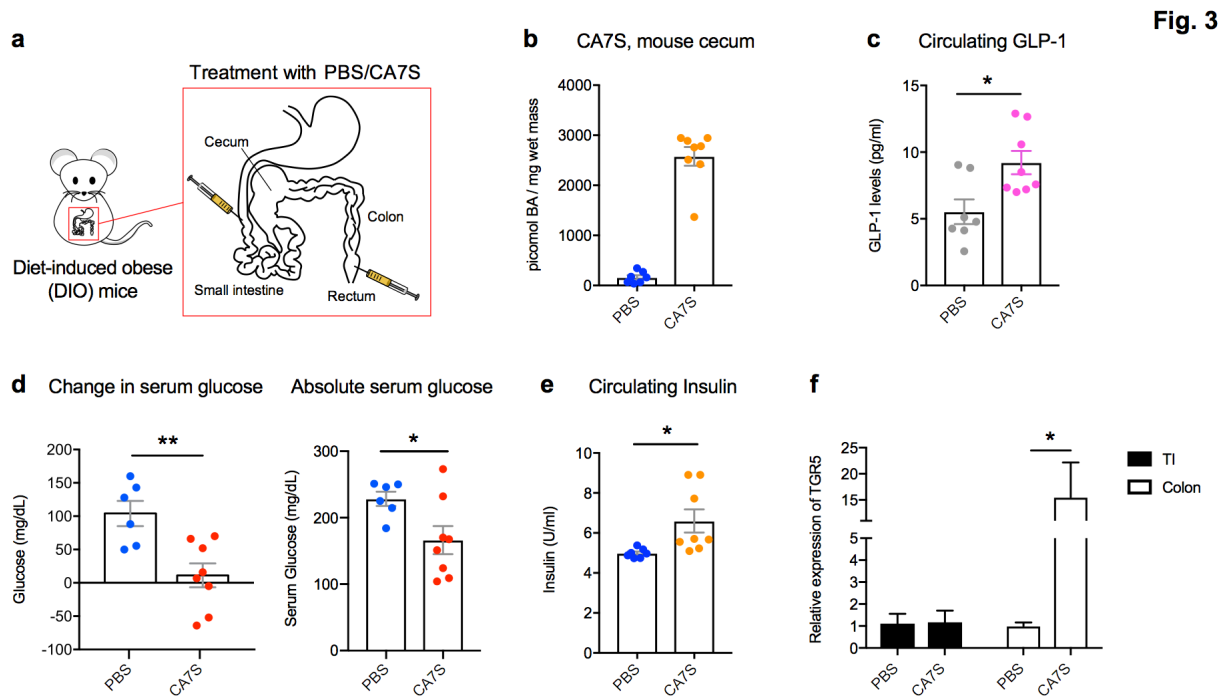
Figure 3. Acute CA7S administration induces GLP-1 and reduces serum glucose levels in vivo

a, Schematic of acute treatment wherein anesthetized DIO mice were treated with PBS or CA7S via duodenal and rectal catheters. **b**, Concentration of CA7S in mouse cecum 15 minutes after treatment with PBS or CA7S (PBS, n=7; CA7S, n=8 mice per group). **c-e**, CA7S-treated mice displayed increased GLP-1 (**c**), reduced blood glucose levels (**d**), and increased blood insulin levels (**e**) compared to PBS-treated mice. (For **c** and **e**, PBS, n=7; CA7S, n=8 mice per group, (**c**) *p=0.012, (**e**) *p=0.023, Welch's t test. For **d**, PBS, n=6; CA7S, n=8 mice per group, **p=0.0043, *p=0.033, Student's t test). **f**, CA7S treatment in the intestine induced TGR5 expression in the colon but not in the terminal ileum (TI) (*p=0.035, Welch's t test). All data are presented as mean ± SEM.

26

Fig. 4
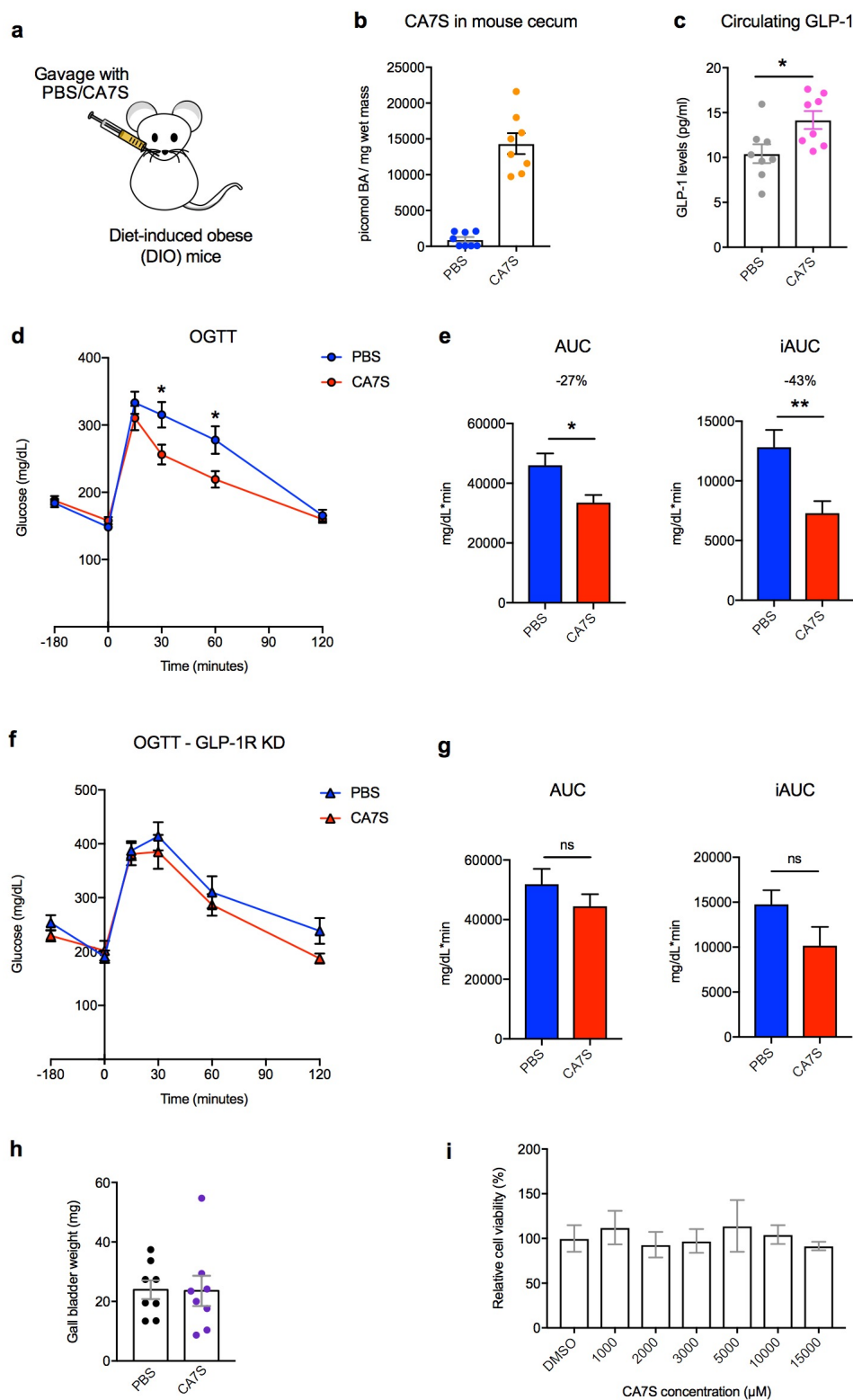
625

626 **Figure 4. CA7S gavage induces GLP-1 and improves glucose tolerance in vivo via GLP-1R**

627 **a**, Schematic of treatment of DIO mice with either PBS or CA7S via oral gavage. **b**, Concentration

628 of CA7S in mouse cecum 5 hours after PBS or CA7S gavage. **c**, CA7S mice displayed increased

629 GLP-1 levels 5 hours post-gavage (For **b** and **c**, n=8 mice per group, *p=0.021, Welch's t test).

630 **d,e**, DIO mice treated with CA7S (100 mg/kg) displayed increased glucose tolerance compared

631 to vehicle-treated mice 3 hours post-gavage as determined by an oral glucose tolerance test

632 (OGTT) (n=11 mice per group). **d**, Glycemic curves during OGTT (*p=0.023, Student's t test). **e**,

633 Corresponding blood glucose AUC and iAUC were significantly reduced in CA7S-treated mice

634 (AUC *p=0.011, iAUC **p=0.004, Student's t test). **f,g**, On day 3 after treatment with lentiviral

635 shRNA targeting GLP-1 receptor (GLP-1R), CA7S (100 mg/kg) or PBS was administered, and 3

636 hours later, an OGTT was performed (n=7 mice per group). **f**, Glycemic curves during OGTT (ns

637 = not significant, 30 min p=0.49, 60 min p=0.53, 120 min p=0.07, Student's t test). **g**,

638 Corresponding blood glucose AUC and iAUC were not significantly different in CA7S- or PBS-

639 treated mice in which the GLP-1R had been knocked down (ns = not significant, AUC p=0.266,

640 iAUC p=0.1, Student's t test). **h**, CA7S treatment does not induce gallbladder filling in mice (n=8

641 mice per group, not significant, p=0.95, Welch's t test). **i**, Percentage cell viability upon treatment

642 of Caco-2 cells with CA7S in vitro ($\geq$3 biological replicates per condition, not significant, $p \geq 0.97$

643 one-way ANOVA followed by Dunnett's multiple comparisons test). All data are presented as

644 mean ± SEM.

645

646

647 **Table 1. Cholic acid-7-sulfate concentration in indicated tissues and blood**

Treatment	Tissue/blood	CA7S concentration (mean ± SEM)
DIO mice; sham surgery	Cecum	1726 ± 267 pmol/mg
	Liver	0.12 ± 0.04 pmol/mg

	Portal vein	n.d.
	Systemic blood	n.d.
DIO mice; sleeve gastrectomy	Cecum	2661 ± 331 pmol/mg
	Liver	0.27 ± 0.04 pmol/mg
	Portal vein	n.d.
	Systemic blood	n.d.
DIO mice; enteral PBS	Cecum	161.1 ± 46.4 pmol/mg
	Portal vein	0.07 ± 0.06 pmol/mg
	Systemic blood	n.d.
DIO mice; enteral CA7S	Cecum	2577 ± 185 pmol/mg
	Portal vein	6.13 ± 2.11 pmol/mg
	Systemic blood	0.5 ± 0.2 pmol/μl
DIO mice; PBS gavage	Cecum	947 ± 349 pmol/mg
	Portal vein	n.d.
	Systemic blood	n.d.
DIO mice; CA7S gavage	Cecum	14345 ± 1451 pmol/μl
	Portal vein	13.2 ± 7.7 pmol/μl
	Systemic blood	n.d.

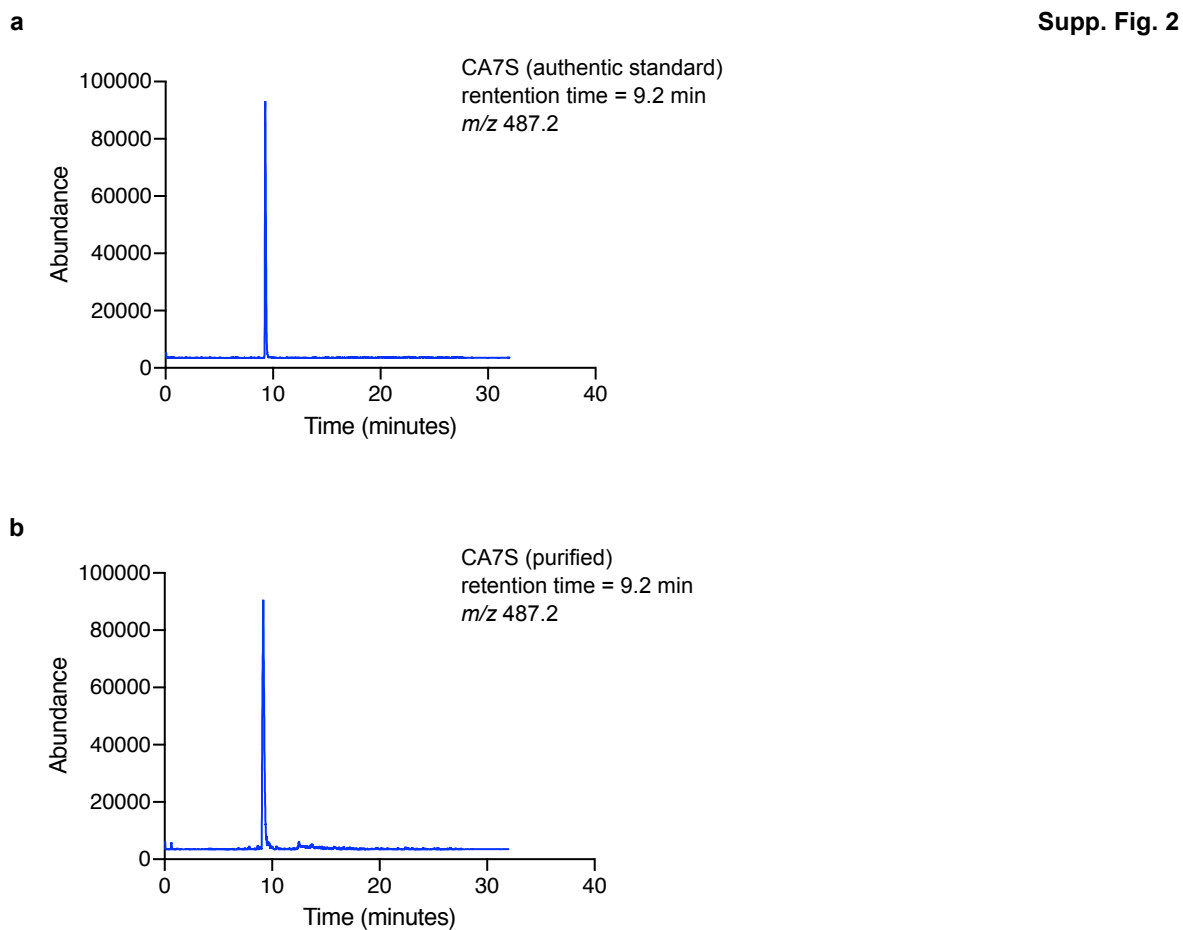648   n.d. not detected, all data are presented as mean ± SEM.

649

29
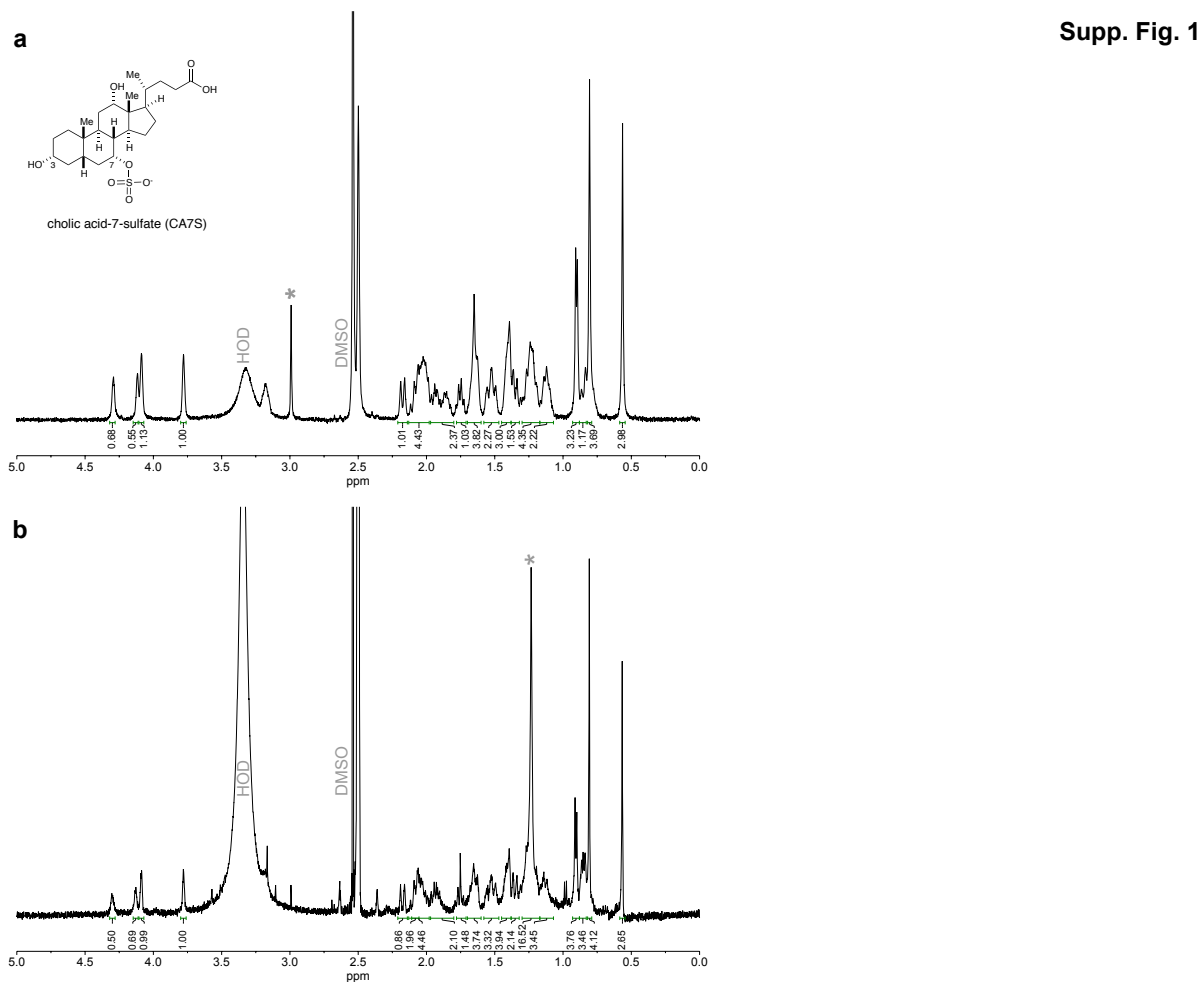
Supplementary Figure 1. NMR of cholic acid-7-sulfate

a, ^{1}H NMR of authentic sample of cholic acid-7-sulfate (Cayman Chemical). **b**, ^{1}H NMR of CA7S purified from the cecal contents of SG mice. Signals between 3.7 to 4.4 ppm are diagnostic of CA7S. Impurities are denoted by asterisks.
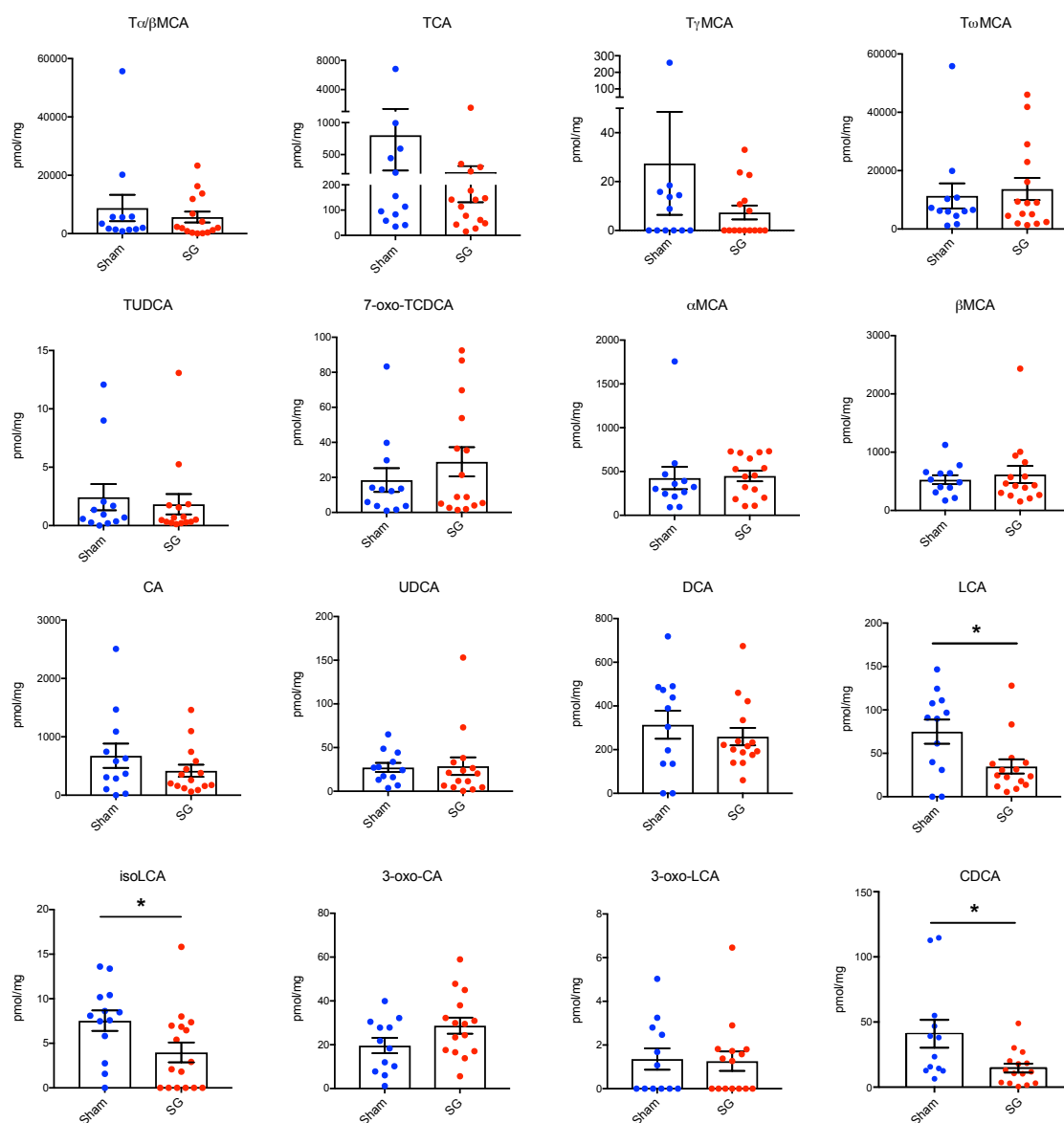
a

Supp. Fig. 2

CA7S (authentic standard)
rentention time = 9.2 min
m/z 487.2

b

CA7S (purified)
retention time = 9.2 min
m/z 487.2

Supplementary Figure 2. UPLC-MS analysis of cholic acid-7-sulfate

a, Commercially available cholic acid-7-sulfate (Cayman Chemical) and **b**, CA7S purified from the cecal contents of SG mice have the same mass (*m/z* 487.2) and elute at 9.2 minutes.
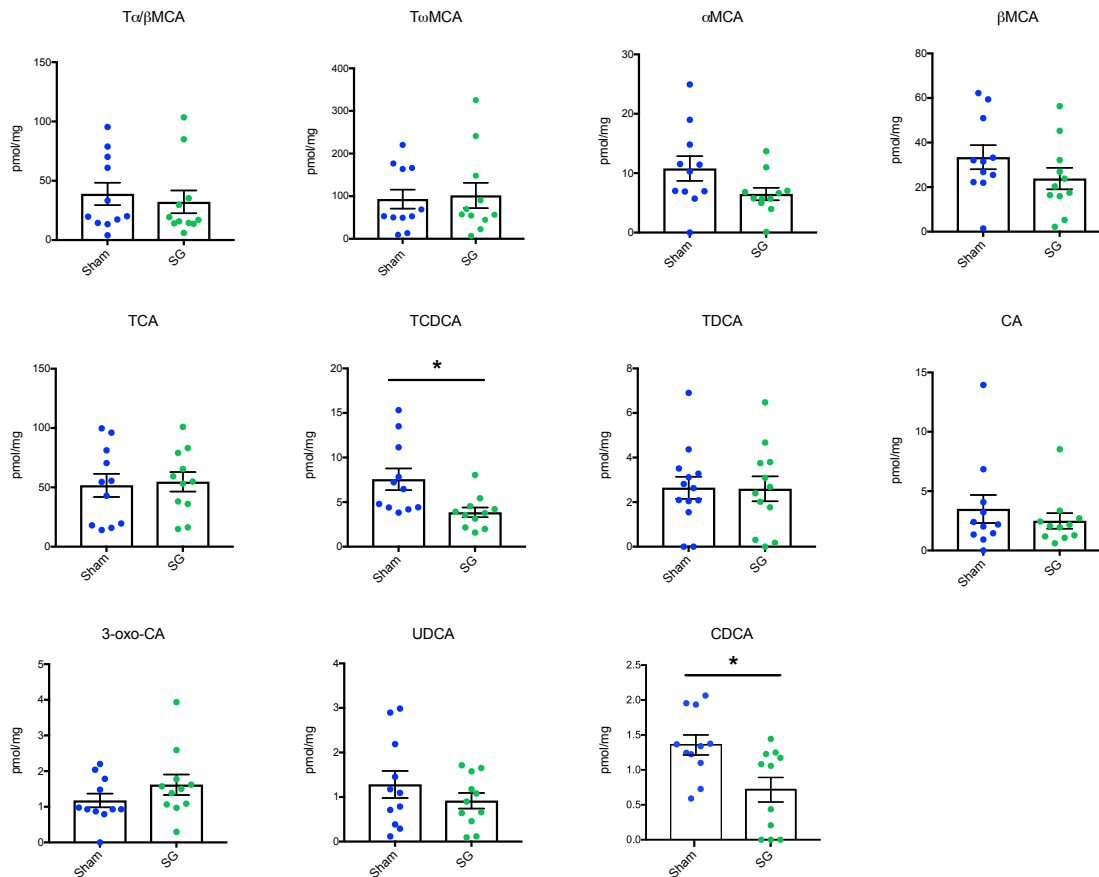
659

Supplementary Figure 3. Bile acid concentrations in cecal contents of mice post-sham or post-SG. Cecal contents were collected from sham or SG mice 6 weeks post-op and bile acids were quantified using UPLC-MS (sham, n=12, SG, n=15, data not marked with asterisk(s) are not significant). All bile acids with measurable concentrations above the limit of detection are shown. Tα/βMCA, tauro-alpha- and tauro-beta-muricholic acid, *p*=0.537; TCA, tauro-cholic acid, *p*=0.325; TγMCA, tauro-gamma-muricholic acid, *p*=0.365; TωMCA, tauro-omega-muricholic acid, *p*=0.685;

32

666　TUDCA, tauro-ursodeoxycholic acid, *p*=0.672; 7-oxo-TCDCA, 7-oxo-tauro-chenodeoxycholic

667　acid *p*=0.34; αMCA, alpha-muricholic acid, *p*=0.874; βMCA, beta-muricholic acid, *p*=0.595; CA,

668　cholic acid, *p*=0.287; UDCA, ursodeoxycholic acid, *p*=0.854; DCA, deoxycholic acid, *p*=0.481;

669　LCA, lithocholic acid, **p*=0.023; isoLCA, isolithocholic acid **p*=0.024; 3-oxo-CA, 3-oxo-cholic acid,

670　*p*=0.087; 3-oxo-LCA, 3-oxo-lithocholic acid, *p*=0.793; CDCA, chenodeoxycholic acid, **p*=0.036,

671　Welch's t test. All data are presented as mean ± SEM.

672

Supp. Fig. 4

673

674　**Supplementary Figure 4. Bile acid concentrations in livers of mice post-sham or post-SG.**

675　Livers were collected from sham or SG mice 6 weeks post-op and bile acids were quantified using

676　UPLC-MS (n=11 per group, data not marked with asterisk(s) are not significant). All bile acids

677　with measurable concentrations above the limit of detection are shown. Tα/βMCA, tauro-alpha-

33

678   and tauro-beta-muricholic acid, *p*=0.625; TωMCA, tauro-omega-muricholic acid, *p*=0.822; αMCA,

679   alpha-muricholic acid, *p*=0.085; βMCA, beta-muricholic acid, *p*=0.203; TCA, tauro-cholic acid,

680   *p*=0.815; TCDCA, tauro-chenodeoxycholic acid, *p=0.015; TDCA, tauro-deoxycholic acid,

681   *p*=0.947; CA, cholic acid, *p*=0.468; 3-oxo-CA, 3-oxo-cholic acid, *p*=0.22; UDCA, ursodeoxycholic

682   acid, *p*=0.314; CDCA, chenodeoxycholic acid, *p=0.023, Welch's t test. All data are presented as

683   mean ± SEM.

684

Supp. Fig. 5
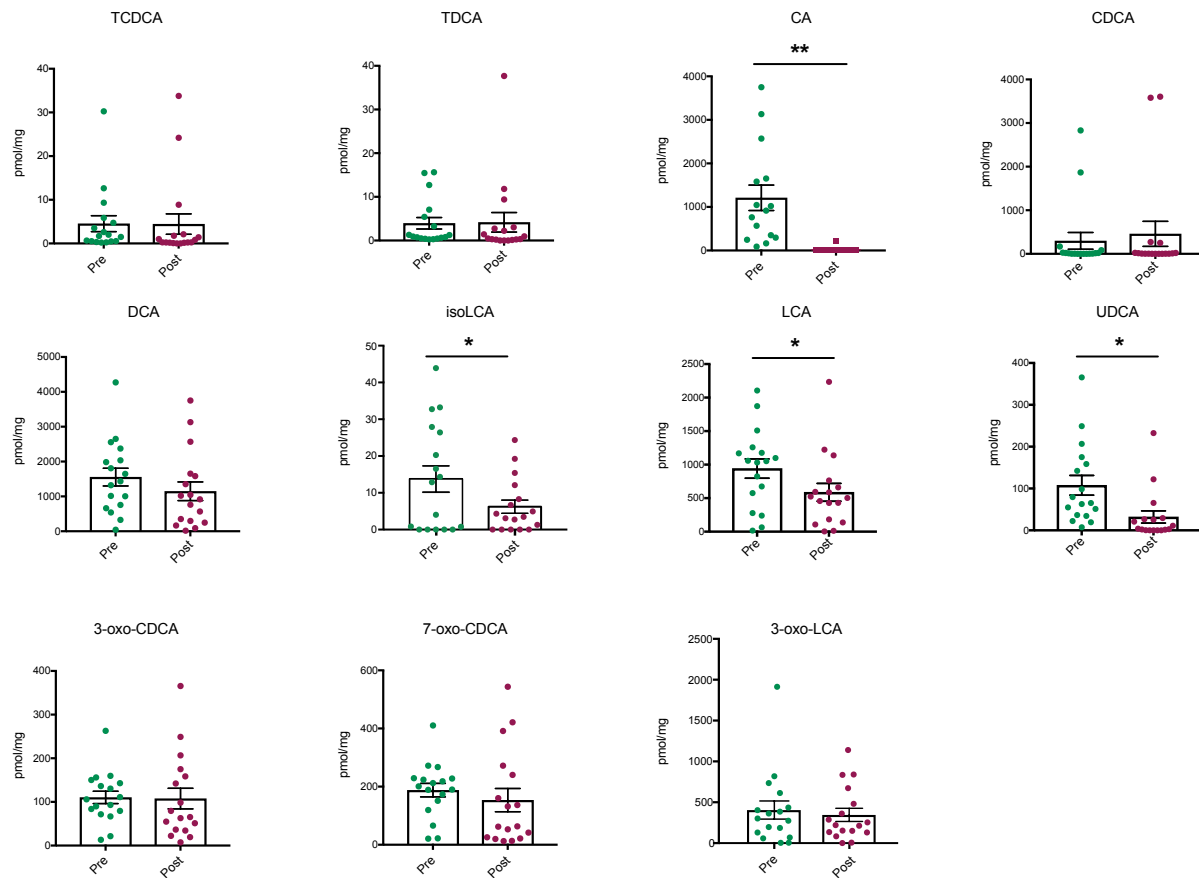
685

686   **Supplementary Figure 5. Bile acid concentrations in feces of human patients pre-SG or**

687   **post-SG.**

688   Feces were collected from patients pre-op or ~5 weeks post-op and bile acids were quantified

689   using UPLC-MS (n=17 patients, median 36 days after surgery, data not marked with asterisk(s)

690   are not significant). All bile acids with measurable concentrations above the limit of detection are

691   shown. TCDCA, tauro-chenodeoxycholic acid, p=0.973; TDCA, tauro-deoxycholic acid, p=0.933;

692   CA, cholic acid, **p=0.001; CDCA, chenodeoxycholic acid, p=0.525; DCA, deoxycholic acid,

693   p=0.135; LCA, lithocholic acid, *p=0.014; isoLCA, iso-lithocholic acid, *p=0.032; UDCA,

694   ursodeoxycholic acid, *p=0.022; 3-oxo-CDCA, 3-oxo-chenodeoxycholic acid, p=0.921; 7-oxo-

695   CDCA, 7-oxo-chenodeoxycholic acid, p=0.477, 3-oxo-LCA, 3-oxo-lithocholic acid, p=0.563,

696   paired t test. All data are presented as mean ± SEM.

697

Supp. Fig. 6
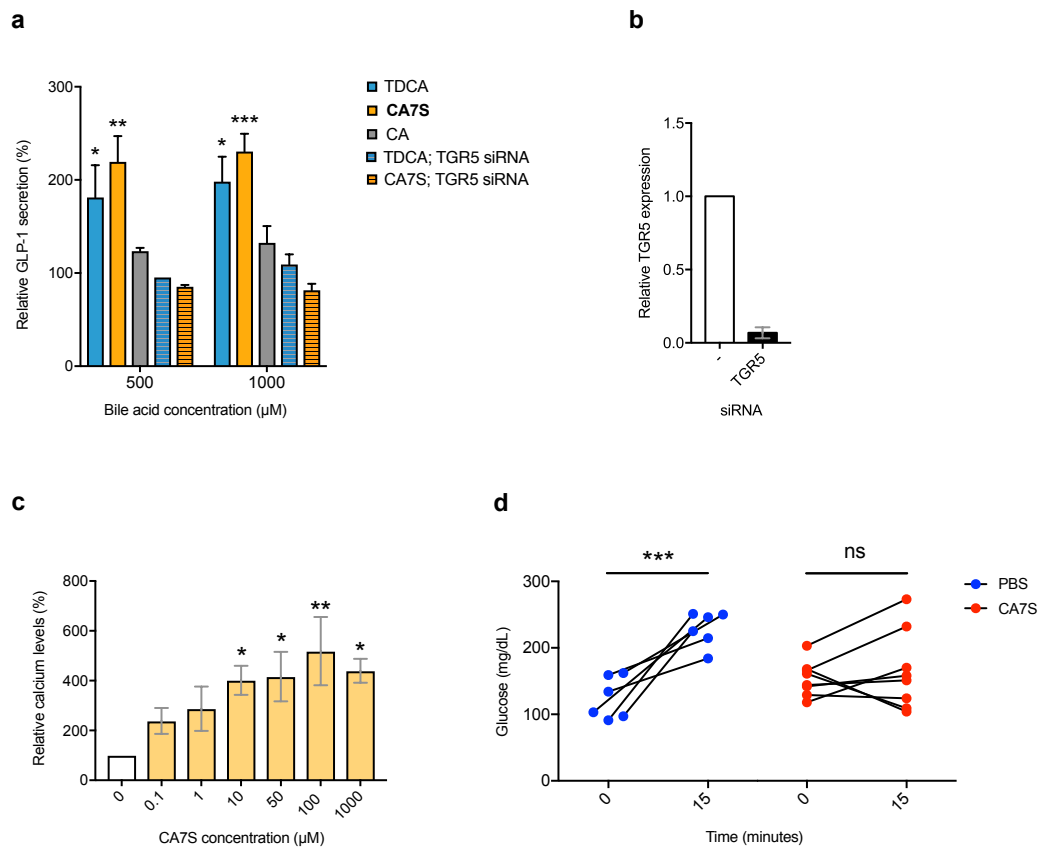
699   **Supplementary Figure 6. CA7S activates TGR5, induces GLP-1 secretion, and reduces**

700   **systemic glucose levels**

701   **a**, CA7S induced secretion of GLP-1 in NCI-H716 cells compared to both CA and the known

702   TGR5 agonist, TDCA. siRNA-mediated knockdown of TGR5 abolished GLP-1 secretion (≥ 3

703   biological replicates per condition, *p=0.027-0.04, **p=0.003, ***p=0.0007, one-way ANOVA

704   followed by Dunnett's multiple comparisons test). **b**, Quantitative real time PCR analysis of

705   expression of human TGR5 in TGR5 siRNA and negative (-) siRNA-treated NCI-H716 cells for

706   Fig. 2g and Supplementary Fig. 6a. **c**, CA7S induced an increase in intracellular calcium levels in

707   NCI-H716 cells (≥ 3 biological replicates per condition, *p=0.018-0.041, **p=0.003, one-way

708   ANOVA followed by Dunnett's multiple comparisons test). **d**, In vivo change in serum glucose

709   upon treatment with PBS and CA7S (PBS, n=6; CA7S, n=8 mice per group, ***p=0.0001, ns=not

710   significant p=0.63, paired t test). All data are presented as mean ± SEM.

Supp. Fig. 7
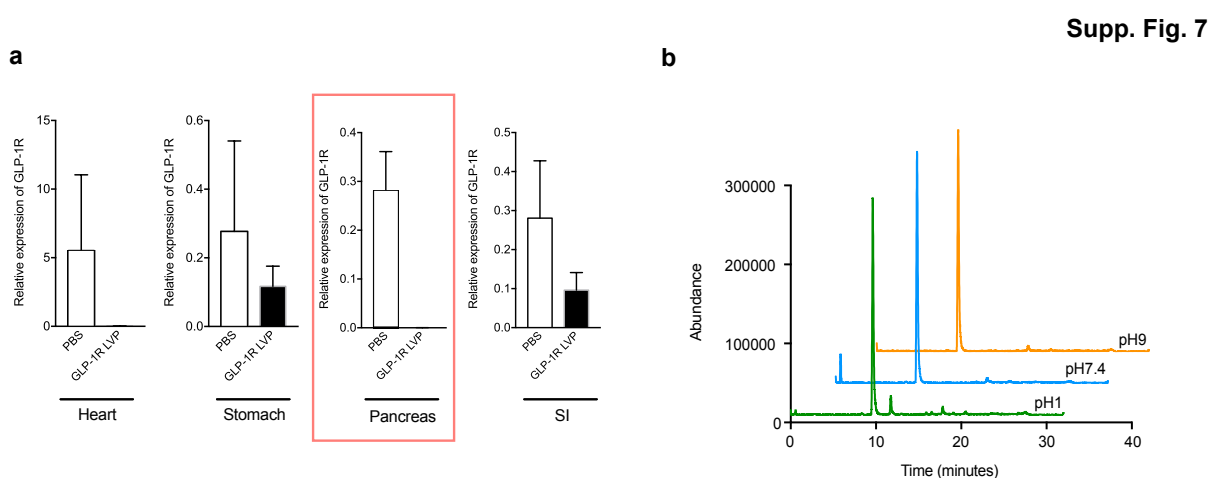
711

712   **Supplementary Figure 7. GLP-1R shRNA knockdown efficiency and stability of CA7S**

713   **a**, Quantitative real time PCR analysis in mice corresponding to Fig. 4f and 4g. Animals were

714   injected with lentiviral shRNA targeting GLP-1R or PBS. Expression of mouse GLP-1R in

715   indicated tissues of mice was measured following OGTT, which was performed 3 days post-

716   injection (SI = small intestine, PBS, n=2; GLP-1R LVP shRNA n=14). **b**, UPLC-MS traces of CA7S

36

717 after incubation at 37 °C in buffer at the indicated physiological pHs. All data are presented as

718 mean ± SEM.

719